

Research Article

Efficacy of Multiseason Sentinel-2 Imagery for Classifying and Mapping Grassland Condition

Diego R. Guevara-Torres , José M. Facelli , and Bertram Ostendorf 

Department of Ecology and Evolutionary Biology, University of Adelaide, Adelaide 5005, SA, Australia

Correspondence should be addressed to Diego R. Guevara-Torres; diego.guevara@adelaide.edu.au

Received 1 June 2023; Revised 17 January 2024; Accepted 21 February 2024; Published 8 March 2024

Academic Editor: Sangsoo Lim

Copyright © 2024 Diego R. Guevara-Torres et al. This is an open access article distributed under the Creative Commons Attribution License, which permits unrestricted use, distribution, and reproduction in any medium, provided the original work is properly cited.

Assessing the condition of ecosystems is imperative for understanding their degree of degradation and managing their conservation. The increasing availability of remote sensing products offers unprecedented opportunities for mapping vegetation with high detail and accuracy. However, mapping complex ecosystems, like grasslands, remains challenging due to their heterogeneity in vegetation composition and structure. Furthermore, degraded ecosystems affected by invasive vegetation present different condition levels within vegetation classes, limiting the accuracy of classifications and condition assessment. Here, we evaluated the capacity of Sentinel-2 multispectral time series imagery as an input for classifying different levels of cover within a vegetation class to detect the subtle differences needed to assess the condition of degraded ecosystems. Our study was conducted in the iron-grasslands of South Australia, a perennial tussock grassland dominated by iron-grasses (*Lomandra* spp.) and severely affected by invasive annual grasses. We developed random forest models to discriminate classes defined by the cover of iron-grasses, wild oats (*Avena barbata*), and woodland (training points = 250). We tested the importance of data seasonality, spatial resolution, spectral bands, and vegetation indices. The combination of spatial, temporal, and spectral detail produced the best classification results. Random forest classifications performed best at 10 m resolution, suggesting that detailed resolution outweighs spectral detail for discriminating vegetation patterns in systems with high spatial heterogeneity. The model at 10 m resolution combining all periods and all variables (spectral bands and vegetation indices) produced a mean kappa coefficient of 56% and a mean overall accuracy of 67%. The dry season imagery and vegetation indices emerged as the most informative, suggesting that vegetation classes presented different phenological properties critical for their discrimination. Our study contributes to mapping complex ecosystems, facilitating the discrimination of different levels of condition in grasslands degraded by invasive species, and thus benefits the conservation of native grasslands and other ecosystems.

1. Introduction

There is an increasing demand to develop accurate maps of vegetation conditions for biodiversity conservation and landscape management [1–3]. Remote sensing methods have been widely used in vegetation mapping to provide comprehensive assessments at broad spatial and temporal scales [4, 5]. The most prominent mapping approach is the classification of remotely sensed imagery into discrete thematic classes to represent vegetation in an area of interest [6, 7]. Most classification techniques are based on the canopy reflectance capture in the electromagnetic spectrum by satellite sensors [8]. Reflectance can be sensitive to plant variation in biochemical and biophysical variables [9]. Thus, differences in

phenological properties between plant species provide the opportunity to discriminate classes in multitemporal datasets [10]. Several modeling techniques correlate spectral signatures to referenced vegetation site-based data at certain phenological stages [11]. Among these techniques, the machine learning approaches have become a trending method due to their flexibility in classifying complex classes without considering statistical assumptions for data distribution [12]. The recent development of fine spatial, spectral, and temporal resolutions in satellites has improved machine learning classifications to unprecedented levels. However, most classifications have been conducted in agricultural landscapes, forests, and woodland, leaving a variety of remote scenarios with a higher level of vegetation complexity to be tested [7].

The random forest (RF) algorithm is a popular machine learning classifier for remote sensing classifications. It has the capacity to handle high-dimensional data and produce accurate classifications in complex environments [13]. By producing a high number of decision trees, the RF algorithm is less sensitive to the quality of training samples and overfitting [14]. The RF algorithm also employs training samples encompassing a wide variety of data, including spectral bands and vegetation indices [15]. In recent years, the emergence of open-source high spatiotemporal and spectral resolution imagery has shown promising results for RF land cover classifications [6, 7]. The twin platform Copernicus Sentinel-2 provides open-source imagery with a high resolution (10–60 m) and short temporal revisit time (5 days), facilitating the construction of dense time series over large spatial extents [16–18]. Among Sentinel-2 bands, the red-edge bands (670–760 nm) are highly sensitive to the leaf chlorophyll content and are effective tools for discriminating vegetation classes [19, 20]. Employing Sentinel-2 imagery in RF classifications has shown successful outcomes in agricultural lands [21], forests [15], wetlands [22, 23], scrubland [7], and grasslands [24–26]. However, classification accuracy is limited by plant community complexity in composition and structure [27].

Native grasslands are diverse ecosystems characterized by high spatial heterogeneity. Grassland vegetation is composed of graminoids and several interspersed herbaceous species that are not always distinguishable, even at high spatial and spectral resolutions [28, 29]. Temporal and spatial dynamics such as rainfall seasonality and physiochemical soil properties affect vegetation composition and structure, leading to discontinuous plant cover [30]. Temperate grasslands, in particular, present dominant perennial and annual graminoids whose phenological characteristics are strongly influenced by rainfall seasonality, increasing the temporal heterogeneity [31]. Furthermore, invasive exotic species severely impact most temperate grasslands, presenting heterogeneity in the proportions of native and exotic species [32]. Consequently, degraded grasslands exhibit a mosaic of patches with different levels of degradation, thus complicating the detection of patterns in vegetation composition that ultimately lead to the dominance of exotic species.

The detection of subtle patterns in plant communities is required for the assessment of grassland conditions. Compositional indicators, such as the cover of dominant native vegetation, can facilitate the assessment of grasslands condition by contrasting undisturbed and disturbed vegetation patches [4]. Recent studies have combined multiseasonal information with phenological properties to improve the separation of patches dominated by native or invasive species [10, 25, 26, 33]. However, due to the small size of grassland species and high heterogeneity in mixed patches (native and exotic species), most classifications use coarse vegetation classes [7]. As a result, classifications often lack information on the level condition inside classes in terms of the proportion between native and invasive species. Defining classes that represent different levels of condition of a plant community based on the presence or cover of a

dominant native species could improve the assessment of grasslands impacted by invasive species. Linking information on the cover of dominant native species with the spatial resolution of open-source satellite imagery can enhance our ability to detect patterns in vegetation communities, providing a more nuanced and comprehensive understanding of grassland condition across time and space.

We aim to explore the suitability of Sentinel-2 time-series data for characterizing the condition of temperate grasslands, defined by the cover of a dominant native perennial graminoid. Sentinel-2 imagery was selected because it provides high temporal and spatial resolution with careful spectral calibration and consistency, which facilitates the applicability of this study in space and time. Here, we provide an RF classification of a complex native grassland invaded by exotic annual grasses. This study focuses on the Iron-grass Natural Temperate Grassland of South Australia (Iron-grasses lands henceforth), a vegetation type dominated by slow-growing large tussock graminoids known as iron-grasses (*Lomandra* spp.) and severely affected by invasive species [34]. Our objectives are to (1) assess if Sentinel-2 time series can be used to discriminate grassland classes defined by iron-grass tussock cover and (2) test the importance of data seasonality, spatial resolution, and whether adding spectral bands and/or vegetation indices would improve classifications.

2. Materials and Methods

2.1. Study Area. The study area (Poonthie Ruwe Conservation Park) covers over 245 ha (35.2983°S, 139.4897°E), about 90 km SE of Adelaide (Figure 1). The park is located in the Mediterranean-type climate region of South Australia, characterized by dry summers (December–February) that are warm to hot and wet winters (June–August) that are mild to cold [35]. Mean daily temperature ranges between 21.3°C in February and 10.4°C in July (Tailem Bend weather town station ID: 95818), with an average annual rainfall of 353.6 mm from 1991 to 2020 recorded by the Australian Bureau of Meteorology. The Poonthie Ruwe Conservation Park represents one of the largest remaining iron-grass grassland patches in South Australia. The study area presents a relatively flat terrain with shallow loam soils over a calcrete rock layer that is frequently exposed. The northern section of the study area was used for sheep grazing before the area was turned into a conservation park in 2003. Graminoids dominate most of the area, with sparse southern cypress pine (*Callitris gracilis*) and eucalyptus woodland to the south. Tussocks of *Lomandra effusa* are present across the area, with greater numbers in the south section. The area is affected by the invasion of wild oats (*Avena barbata*), a common annual weed in the region, that is present across the study site. Other weeds like horehound (*Marrubium vulgare*) can be found across the area in lesser abundance.

2.2. Field Data Collection. In 2020 (May–July), we located 250 training points by traversing the study area and assessing the vegetation approximately every 30 m. Areas with large extents of calcrete rock were avoided to reduce the variability in the spectral reflectance of vegetation. At each point, we

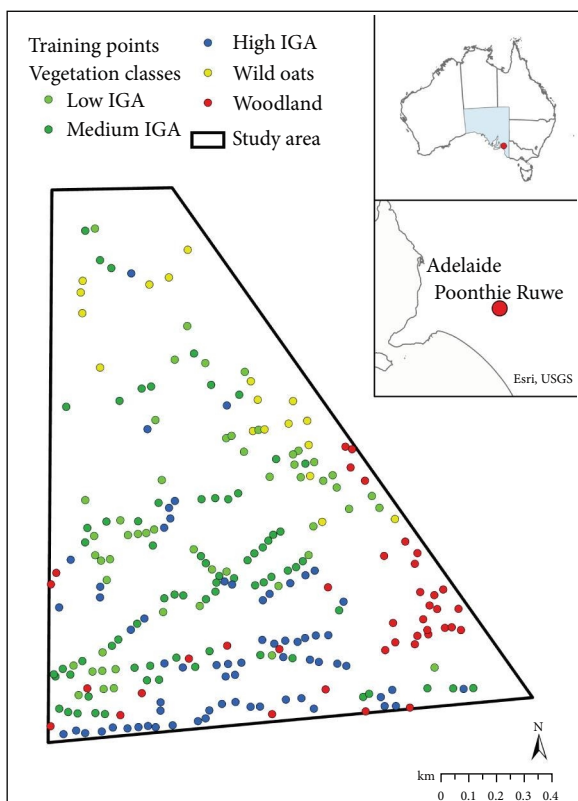


FIGURE 1: Poonthie Ruwe Conservation Park. Training points are colored by vegetation classes. Wild oats in yellow, Low IGA in light green, medium IGA in green, high IGA in blue, and woodland in red.

assessed the vegetation and assigned a class according to the dominant vegetation within a radius of 10 m. We considered five vegetation classes that included iron-grass grasslands with three levels of condition, patches dominated by wild oats (with no iron-grass present) and woodland. Iron-grass grassland condition classes considered the iron-grass abundance (IGA) as the number of tussocks (average size: within 10 m of the training point and were defined as low IGA: 1–30, medium IGA: 31–100, and high IGA: >100). We only observed counts without collecting location data for individual tussocks. We also considered the vegetation classes wild oats and woodland. We collected 18 points for wild oats, 52 for low IGA, 73 for medium IGA, 68 for high IGA, and 39 for woodland. The shape of the field observations is a circular area ($r = 10$ m). This area is similar to the pixel size of Sentinel-2 (10 and 20 m) and hence facilitates the link to individual raster cells. The datasets for RF model training are generated by extracting satellite imagery at the centroids of the field observations. Model predictions produce rasters at 10 or 20 m pixel sizes, respectively.

2.3. Analysis Overview. In order to evaluate the potential of multitemporal Sentinel-2 imagery to identify subtle patterns of plant community composition, we use our field observations as reference (Figure 1). The guiding principle was to quantitatively evaluate how well satellite imagery can be used to discriminate plant community differences. We used RF

classification models with different combinations of spectral bands, vegetation indices, and different time periods. The different RF models are called “scenarios.” Scenarios were repeated at two spatial resolutions (10 and 20 m), allowing us to assess spatial, spectral, and temporal satellite imagery characteristics.

For each scenario, we created $k = 40$ different random sets, splitting observations into training (70%) and testing (30%) points to be used in the RF models. We applied the Boruta algorithm to each set to simplify the model and obtain the best RF classification outcomes. In order to assess the performance of the scenarios, we averaged kappa and overall accuracy across the 40 classifications done for each scenario (Figure 2).

2.4. Remote Sensing Data. Sentinel-2 images were acquired from the European Space Agency Copernicus Open Access Hub using the packages RGISTools and sen2r in R software [36]. We downloaded level-2A, which comprises image orthorectification, along with atmospheric and slope corrections [37]. Mosaics were masked to the study area polygon in order to be filtered with a cloud coverage threshold of 0.1% and shadow masks provided by level-2A images, resulting in a RasterStack of 35 dates from 2020. This process was followed by a visual inspection to identify cloud, dust, or smoke-affected imagery, rejecting eight dates. We considered spectral bands at 10 and 20 m resolutions (Table 1). The red-edge bands (B5, B6, and B7) and short-wave infrared (SWIR) bands (B11 and B12) were resampled from 20 to 10 m resolution, using the nearest neighbor method from the package Raster in R software (Table 1).

We used seven spectral indices (Table 2). These included the normalized difference vegetation index (NDVI) and the enhanced vegetation index 2 (EVI2), two indices commonly used in vegetation classification analysis [38, 39]. We also included indices calculated with the red-edge bands and SWIR bands due to their importance for vegetation classification [38, 40]. These included the normalized difference red-edge (NDRE) index, the red-edge enhanced vegetation index 2 (red-edge EVI2), the red-edge chlorophyll index (CIRE), the SWIR ratio, and the normalized difference water index (NDWI). All indices were calculated at both resolutions, employing B8 for the 10 m resolution and B8a for the 20 m scale. The indices employing red-edge bands were calculated with B5, commonly used for red-edge band vegetation indices [7, 25].

2.5. Selection of Dates. To determine key dates that facilitate the discrimination by phenology, we analyzed the separability of the vegetation classes across an NDVI time series from 2020 at a 10 m resolution (Figure 3). NDVI was selected due to its importance as a standard index for vegetation classifications [8, 41]. The time series of NDVI averaged for the vegetation classes revealed three time periods defined as the early dry season (D1), from January to April. The rainy season (R) is from May to October. And the late dry season (D2) is from November to December. We selected two representative dates for each of the three time periods: D1: 2 Jan and 7 March, R: 15 Jul and 14 Aug, and D2: 17 Nov and 27

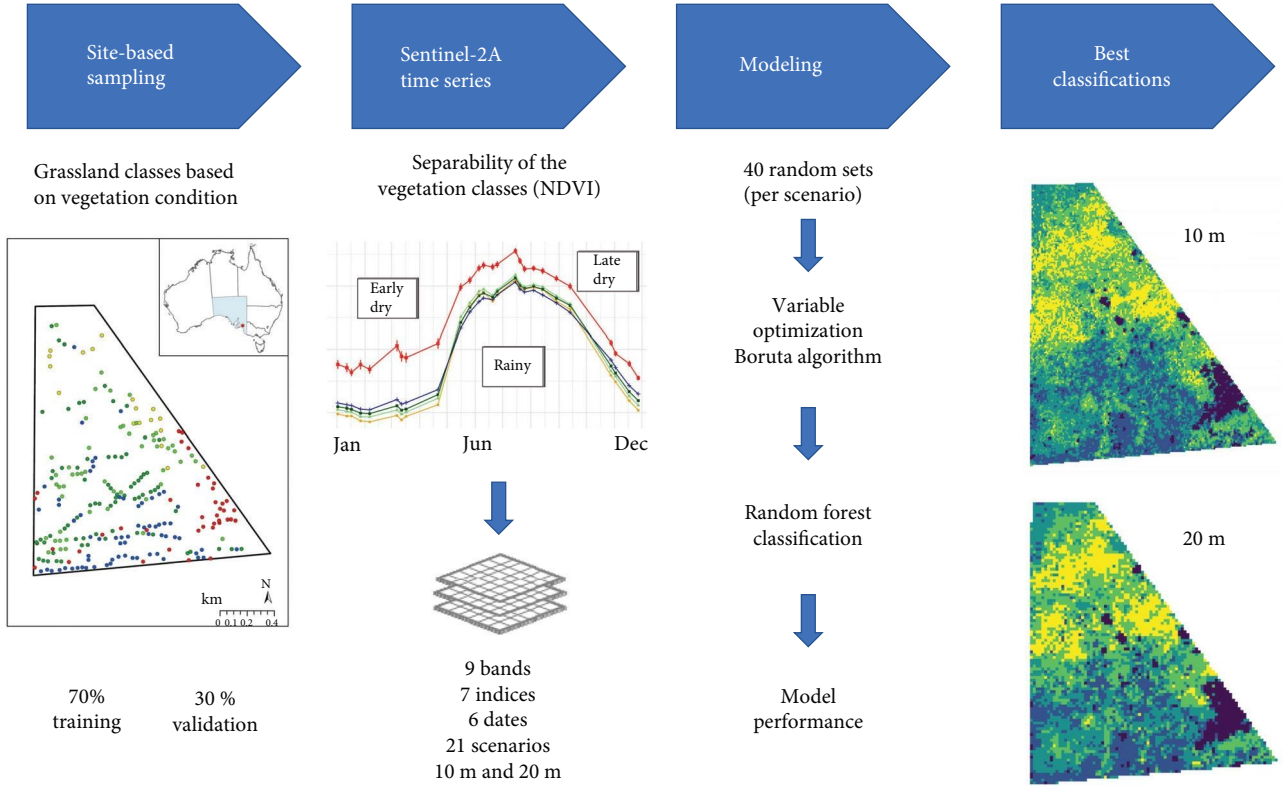


FIGURE 2: Flowchart showing the methodological procedure followed in the study.

TABLE 1: List of spectral bands used in random forest classifications.

Bands	Description	Central wavelength (nm)
B2	Blue	490
B3	Green	560
B4	Red	665
B5, B6, B7	Red edge	705, 740, 783
B8, B8a	Near infrared (NIR)	742,765
B11, B12	Short wave infrared (SWIR)	1,610, 2,190

TABLE 2: List of vegetation indices used in random forest classifications.

Indices	Formula
NDVI	$(\text{NIR} - \text{R}) / (\text{NIR} + \text{R})$
EVI2	$2.5 \cdot (\text{NIR} - \text{R}) / (\text{NIR} + 2.4 \cdot \text{R} + 1.0)$
NDRE	$(\text{NIR} - \text{R}) / (\text{NIR} + \text{R})$
Red-edge EVI2	$2.5 \cdot (\text{NIR} - \text{red edge}) / (\text{NIR} + 2.4 \cdot \text{red edge} + 1.0)$
CIRE	$\text{NIR} / \text{red-edge-1}$
SWIR ratio	$\text{SWIR (B11)} / \text{SWIR (B12)}$
NDWI	$(\text{NIR} - \text{SWIR (B11)}) / (\text{NIR} + \text{SWIR (B11)})$

Nov. Dates were enumerated from 1 to 6 according to the calendar.

2.6. Classification Scenarios. The full dataset contains nine bands and seven indices at six dates and two spatial resolutions ($16 \times 6 \times 2$ spatial data layers). We grouped these into

21 different scenarios based on combinations of spectral bands and vegetation indices at selected time periods (Table 3). All scenarios were developed at 10 and 20 m resolutions.

2.7. Modeling Process and Model Performance. We used the RF Classifier in conjunction with the Boruta algorithm for variable confirmation. The RF classifier is a supervised machine learning algorithm employed for classification and regression, which integrates multiple decision trees whose results are combined into one final result [42]. Decision trees are a type of model that employs randomly selected training samples to learn the characteristics of the classes that the model will be predicting. Prior to the RF model execution, we conducted a Boruta-based variable selection to reduce the dimensionality of data due to the large number of variables considered. Boruta is a feature selection wrapper algorithm that works around classification methods like RF [43]. Boruta computes a statistically significant division between important and irrelevant variables, providing a set of confirmed variables to be used in modeling. Both analyses were conducted in R software, using the packages randomForest and Boruta [43].

For each scenario, we repeatedly selected random subsets of 70% ($n = 175$ training points) of the field observations for training and the remaining 30% ($n = 75$ testing points) for model testing. This process was repeated 40 times for each scenario to reduce any bias caused by the use of a single training point set. Each training subset was employed in the Boruta-based variable selection and subsequent RF modeling training. The trained RF models were applied to

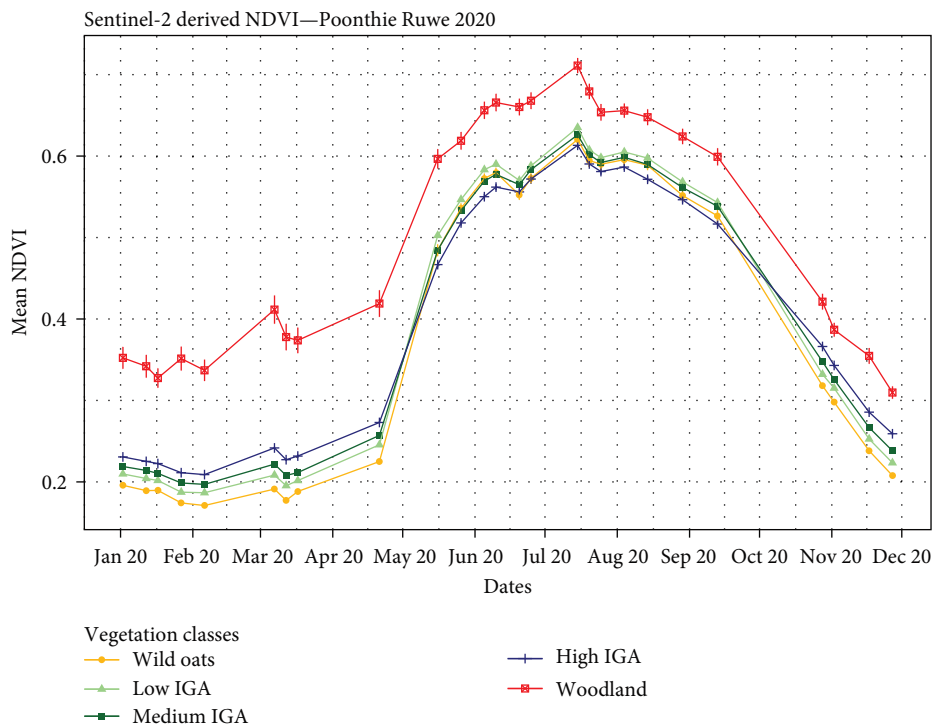


FIGURE 3: Vegetation classes spectral responses to the early dry season (D1), rainy season (R), and late dry season (D2) 2020 time periods.

TABLE 3: Scenarios considered for modeling, based on the combinations of time periods (early dry season D1, the rainy season R, the late dry season D2), bands (B), and vegetation indices (I).

Time periods	Number of dates	Bands (B)	Indices (I)	Number of input variables (k)	Scenario code
D1D2R	6	9	7	96	D1D2R_BI
D1D2R	6	9	—	54	D1D2R_B
D1D2R	6	—	7	42	D1D2R_I
D1D2	4	9	7	64	D1D2_BI
D1D2	4	9	—	36	D1D2_B
D1D2	4	—	7	28	D1D2_I
D1R	4	9	7	64	D1R_BI
D1R	4	9	—	36	D1R_B
D1R	4	—	7	28	D1R_I
D2R	4	9	7	64	D2R_BI
D2R	4	9	—	36	D2R_B
D2R	4	—	7	28	D2R_I
D1	2	9	7	32	D1_BI
D1	2	9	—	18	D1_B
D1	2	—	7	14	D1_I
D2	2	9	7	32	D2_BI
D2	2	9	—	18	D2_B
D2	2	—	7	14	D2_I
R	2	9	7	32	R_BI
R	2	9	—	18	R_B
R	2	—	7	14	R_I

Empty cells refer to the absence of variable.

their corresponding testing subset. To assess the performance of the models, we calculated the mean overall accuracy (MOA) and mean kappa coefficient (MKC) for each of the 21 scenarios at both resolutions (10 and 20 m). We

selected scenario D1D2R_BI, which considered all variables, to discuss the importance of variables (bands and indices) by calculating the mean importance values assigned by the Boruta-based variable selection. We also employed these

Scenario	Number of input variables (k)	Mean number of confirmed variables		Mean overall accuracy (%)		Mean kappa coefficient	
		10 m	20 m	10 m	20 m	10 m	20 m
D1D2R_BI	96	30.5	28.1	67	52	0.56	0.37
D1D2R_B	54	21.5	24.9	54	50	0.4	0.35
D1D2R_I	42	21.3	22.3	66	51	0.55	0.36
D1D2_BI	64	23.7	23.9	65	52	0.54	0.38
D1D2_B	36	16	20	56	48	0.42	0.32
D1D2_I	28	22.5	20.1	64	50	0.53	0.35
D1R_BI	64	24	20.6	61	49	0.49	0.33
D1R_B	36	17.1	21	55	48	0.41	0.32
D1R_I	28	15.2	12.8	60	46	0.48	0.3
D2R_BI	64	24.95	23.3	64	53	0.53	0.38
D2R_B	36	16.5	19.8	54	51	0.39	0.35
D2R_I	28	17.1	15.6	63	48	0.51	0.33
D1_BI	32	16.6	18.1	60	49	0.48	0.34
D1_B	18	12.6	15.5	57	48	0.43	0.31
D1_I	14	10.9	11.6	59	46	0.46	0.3
D2_BI	32	16.9	15.7	62	50	0.49	0.35
D2_B	18	12	12.8	51	49	0.35	0.32
D2_I	14	11.7	10.2	59	46	0.46	0.3
R_BI	32	13.8	13.7	47	42	0.31	0.23
R_B	18	9.9	11.3	44	42	0.26	0.25
R_I	14	10.2	10.5	43	40	0.25	0.2

FIGURE 4: Summary of efficiency metrics for all scenarios at 10 and 20 m resolutions over 40 random forest models. D1, early dry season; D2, late dry season; R, rainy season; B, spectral bands; I, vegetation indices. Mean number of confirmed variables by the Boruta algorithm for all scenarios (colors range from blue (high) to red (low)). Mean overall accuracy (MOA) and mean kappa coefficients (MKC) values for all scenarios (colors range from green (high) to red (low)).

scenarios to discuss the classification accuracy for each vegetation class based on the mean accuracy obtained during the training process. To assess the grassland condition based on our results, we generated classification maps for the scenarios with the highest MKC at each spatial resolution. We discuss the distribution of vegetation classes to identify sections of our study area in good and bad conditions.

3. Results and Analysis

3.1. Model Performance. The highest MKC (0.56) and MOA (67%) were achieved by scenario D1D2R_BI at a 10 m resolution incorporating all available variables: the three time periods, bands, and indices (Figure 4). Similar MKC values were achieved by other scenarios considering the early and late dry seasons (D1D2): D1D2R_I (0.55), D1D2_BI (0.54), and D1D2_I (0.53). At 10 m resolution, scenarios composed of one or both dry seasons performed better (MKC values: 0.35–0.54) than scenarios composed of only the rainy season (MKC values: 0.25–0.31). Using only indices resulted in better MKC and MOA than using only bands. In contrast, the scenarios at 20 m resolution presented low accuracies. The highest MKC (0.38) and MOA (53%) were achieved by the D2R_BI scenario at 20 m

resolution. Scenarios composed of one or both dry seasons performed better (MKC values: 0.3–0.38) than scenarios composed of only the rainy season (MKC values: 0.2–0.25). Using only bands resulted in better performances than using only indices. However, these differences were minimal. Colors are scaled across MOA and MKC columns at each resolution, respectively, providing visual accuracies per scenario.

3.2. Variable Importance. We selected the scenario D1D2R_BI to compare the importance of variables at 10 and 20 m resolution. At 10 m resolution, 21 variables were confirmed as relevant in all 40 randomizations, while in the 20 m scenario, only the number of confirmations was not higher than 24 (Table 4). The NDVI and EVI2 indices presented the highest mean importance values for both scenarios. In the case of the 20 m resolution, the red band, Red-edge EVI2, and CIRE were among the top 10 most important variables. Both scales presented the early dry season (2 Jan, 7 March) as the most important, followed by the late dry season (27 Nov, 17 Nov).

3.3. Vegetation Classes Classification Accuracy. A detailed analysis of the classification accuracy of vegetation classes from scenario D1D2R_BI revealed that mean accuracies

TABLE 4: Top 20 variables with the highest number of confirmations by the Boruta algorithm for scenario D1D2R_BI at 10 and 20 m resolutions for 40 RF models.

D1D2R_BI (10 m)			D1D2R_BI (20 m)		
Variable	Mean number of confirmations (0–40)	Mean Boruta importance	Variable	Mean number of confirmations (0–40)	Mean Boruta importance
ndvi.2	40	12.2	evi2.2	24	7.29
evi2.2	40	12.1	ndvi.2	24	7.13
ndvi.6	40	9.3	evi2.5	24	6.79
evi2.6	40	9.3	ndvi.5	24	6.75
ndvi.1	40	9	cire.2	24	6.62
evi2.1	40	9	ndre.2	24	6.6
evi2.5	40	8.5	red_evi2.2	24	6.55
ndvi.5	40	8.5	SWIR11.2	24	6.23
B.3	40	7.1	R.5	24	5.69
B.2	40	6.8	ndwi.2	23	5.59
G.3	40	6	cire.1	24	5.36
R.5	40	5.8	ndre.1	24	5.35
R.3	40	5.5	red_evi2.1	24	5.35
G.4	40	5.3	red_evi2.5	24	5.15
B.1	40	5.1	cire.5	24	5.13
cire.2	40	5	ndre.5	24	5.09
red_evi2.2	40	4.9	SWIR11.5	23	4.87
ndre.2	40	4.9	RE5.5	20	4.81
R.2	40	4.9	cire.6	20	4.33
evi2.3	40	4.8	red_evi2.6	21	4.33
ndvi.3	40	4.8	ndre.6	21	4.32

Number of confirmations range from 0 to 40. Each variable presents a mean boruta importance value ($n = 40$). Numbers in variables correspond to the image date. 2 Jan = 1, 7 March = 2, 15 Jul = 3, 14 Aug = 4, 17 Nov = 5, and 27 Nov = 6. D1, early dry season; D2, late dry season; R, rainy season; B, spectral bands; and I, vegetation indices.

TABLE 5: Mean overall accuracies of each vegetation class for the D1D2R_BI scenario at 10 and 20 m scales ($n = 40$).

Resolution (m)	Scenario	Wild oats (%)	Low IGA (%)	Medium IGA (%)	High IGA (%)	Woodland (%)
10	D1D2R_BI	51	55	62	75	90
20	D1D2R_BI	40	50	46	58	73

D1, early dry season; D2, late dry season; R, rainy season; B, spectral bands; I, vegetation indices.

were higher in the 10 m scale for all classes (Table 5). Woodland presented the highest mean accuracy for both scales. In the case of the 10 m scale, the accuracy decreased proportionally to iron-grass cover, presenting the lowest accuracy for wild oats. The 20 m resolution also presented wild oats with the lowest accuracy, and all IGA classes had an accuracy lower than 60%.

3.4. Distribution of Grassland Condition. Classification maps for both scales showed similar patterns. Grasslands with better condition (more iron-grass) were located in the south section of the park, while the north central section was the most affected by wild oats. Woodland area was located at the same locations for both scales (Figure 5).

4. Discussion

4.1. Variables Influencing Model Performance. Our results showed that the 10 m resolution outperformed the 20 m resolution in all scenarios. The inherent heterogeneity of

tussock grasslands and the small size of tussocks compared to shrubs or trees could have favored the 10 m bands. Tussocks can present highly variable spatial patterns since fine-scale environmental or resource gradients influence their aggregation [44]. Furthermore, invasive species affect native species increasing patch heterogeneity. Consequently, greater spatial resolutions may imply more variability in the spectral reflectance of vegetation classes. The detail obtained by the 10 m resolution appeared to be efficient for classifying iron-grass grassland classes despite the variability present at different levels of tussock cover. A fine spatial resolution may be necessary to discriminate different levels of cover in heterogeneous systems like grasslands. Employing imagery with higher spatial resolution from drones or commercial satellites could contribute to capturing the heterogeneity of tussock grasslands, but it implies more human and economic resources over time and space.

The multitemporal datasets composed of the three time periods (early and late dry season and rainy season)

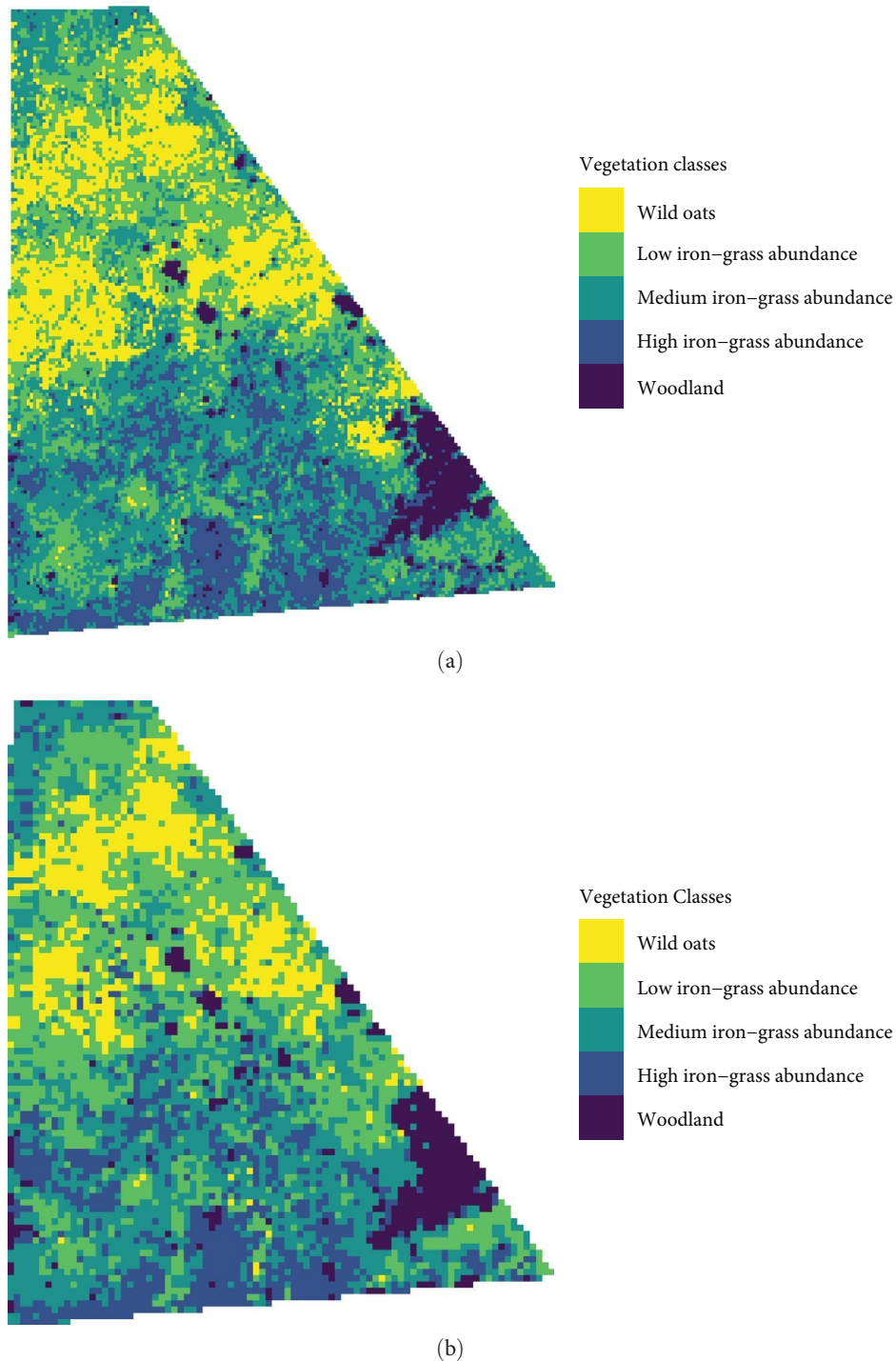


FIGURE 5: (a) Map of vegetation classes derived from the classification of Sentinel-2 time series using a random forest classifier for scenario D1D2R_BI at 10 m resolution. (b) Map of vegetation classes derived from the classification of Sentinel-2 time series using a random forest classifier for scenario D1D2R_BI at 20 m resolution. D1, early dry season; D2, late dry season; R, rainy season; B, spectral bands; I, vegetation indices.

contributed to better performances at both scales. However, excluding the rainy season resulted in similar MOA and MKC, indicating that dry season imagery is key for the discrimination of iron-grasses. High leaf area in all vegetation classes during the rainy season increases homogeneity of reflectance. These results are consistent with the importance of data seasonality for the discrimination of perennial

graminoids reported in other studies [10, 25]. However, the importance of seasonality for grassland classifications may vary depending on the type of climate [45] or the phenological properties of dominant native vegetation and invasive species [46]. In South Australian temperate grasslands, perennial tussocks become more visible during the dry season, contrasting to annual graminoids, which are either

absent or present as dead biomass [47]. Model performance increased with the number of time periods used. The better results obtained by the combinations of all time periods could be linked to the detection of less pronounced phenological differences.

The red-edge band had a surprisingly low performance. Most studies consider the red-edge bands over the RGB or NIR bands for their capacity to capture and record variations in vegetation pigment concentration [40]. However, the red-edge bands have mainly been used in cropland and woodland systems with a more even canopy structure than grasslands [38]. In the case of grasslands, other studies showed that red-edge bands have a limited capacity to discriminate between target vegetation, even when rescaled to 10 m resolution [10, 25].

Our results showed that the number of variables strongly influences model performance. The D1D2R_BI scenario with the maximum (96) number of variables had the best performance with a MOA of 67% at the 10 m scale. Previous studies have reported that multidimensional datasets improve classification accuracy in RF classifications of land types [13, 48]. However, big datasets can contain variables that are of little importance. The Boruta algorithm only kept ~30% of the variables in the D1D2R_BI scenario. Scenarios with smaller datasets than D1D2R_BI had similar MOA and MKC (>60%). Application of the Boruta algorithm improved our results, indicating the presence of redundant variables and the importance of variable reduction in our study. Scenarios considering spectral bands and indices had a better performance at both scales. At 10 m resolution, scenarios based on indices performed better than those using bands, with little improvement in including both. In contrast, at 20 m resolution, scenarios based on bands or indices presented similar performances.

4.2. Variable Selection and Importance. The Boruta algorithm applied to the D1D2R_BI scenario enables analysis of variable importance. The algorithm selected NDVI and EVI2 as the two most important variables for both scales. These indices have been widely used to discriminate crops and woodlands [7]. The importance of other variables differed between scales. The good performance of dry-season RGB bands at 10 m resolution can be explained by the differences in red reflectance of iron-grasses (green vegetation) compared with dead biomass and bare soil. The importance of the green band is related to chlorophyll content differences between vegetation classes [49]. The blue band distinguishes vegetation and soils [50]. Red-edge bands and indices showed less relevance at 10 m but were more important at the 20 m scale scenario. The low performance of red-edge bands at 10 m is likely because they were resampled from 20 m pixel size and thus present lower spatial detail than the other bands.

4.3. Vegetation Classes Detection. The discrimination accuracy of vegetation classes from the D1D2R_BI scenario differed between woodlands and graminoids. The high accuracy (>70%) for woodland at both scales could be related to their distinct spectral signatures and the spatial and temporal homogeneity of woodland patches. In contrast, grassland patches are characterized by a high spatiotemporal heterogeneity, forming

complex vegetation patterns that limit predictive accuracies [7, 27]. Invasive species in degraded environments not only affect the composition of native vegetation but modify the spectral reflectance of vegetation, complicating remote sensing classifications. In our study site, wild oats grow in the spaces between iron-grass tussocks, increasing the vegetation heterogeneity as tussock cover decreases. Wild oats become the dominant vegetation when iron-grass tussocks become sparser. These changes in vegetation composition could have increased the variability in spectral reflectance, especially in classes with lower iron-grass presence. At 20 m resolution, patchiness of iron-grass makes this pattern appear less pronounced, which reduces classification accuracy.

Other sources of heterogeneity across our study could influence classification accuracies. These sources include native and invasive perennial graminoids, young native pines, and exposed calcrete rock layers. Invasive perennial graminoids do not have an extensive cover in our study site but are often present in patches with few iron-grass tussocks. Native perennial species such as the black grass saw-sedge (*Gahnia lanigera*), wallaby grass (*Rytidosperma* spp.), speargrass (*Austrostipa* spp.), and groundsels (*Senecio* spp.) are usually present in good condition areas that present a medium to high iron-grass cover. The spectral similarity between iron-grass and other perennial vegetation can lead to the iron-grass overestimation and misclassification of wild oats. However, the usefulness of the presented classification approach for condition assessment is not substantially impacted because the classes portrayed the dominant vegetation in the system.

4.4. Implementation of Grassland Mapping in Conservation.

This study illustrates a methodology that predicts the distribution of iron-grass grassland condition based on the cover of iron-grass tussocks. We also predict the distribution of patches dominated by wild oats and woodland, facilitating the assessment of degraded patches. Our results show that the south section of Poonthie Ruwe Conservation Park had the best condition, presenting patches with a high cover of iron-grass. In contrast, the north-mid part of the park appeared to be more affected by wild oats and had a low iron-grass cover. The distribution of grassland condition is consistent with the area's grazing history and vegetation surveys conducted by the Department of Environment and Water Resources over the last decade. The analysis proposed in our study can help managers to produce a detailed map of the condition of iron-grass grasslands, enabling the identification of different condition levels and the identification of patches impacted by exotic species.

5. Conclusions

This study has demonstrated the potential of the RF classifier to map iron-grass grassland condition using Sentinel-2 temporal information. We discriminated three classes of iron-grass grassland, facilitating the detection of subtle differences within a vegetation class, which could be used as an indicator of condition in degraded systems. Furthermore, we also discriminated woodland and grassland patches dominated by wild oats, an invasive species of substantial management

concern. The consideration of spatial, temporal, and spectral detail in classification models is relevant for the performance of RF classifications.

RF performed better at 10 m pixel size compared to 20 m, suggesting that higher spatial resolution in the imagery is critical for detecting condition patterns at scales under 30 m. Increasing resolution seems to outweigh the benefits of using higher spectral detail for classifications in systems with high spatial heterogeneity. Consequently, the advantage of red-edge bands (20 m resolution) to detect physiological differences in plants does not improve classification performance in these environments.

Scenarios with multiple datasets that include dry and rainy seasons performed better than single-season and single-date scenarios. The early and late dry seasons were the most informative periods, with minor contributions from the rainy season. The associated vegetation indices were more relevant than spectral bands (including red-edge bands). Vegetation classes presented different phenological properties critical to their discrimination, confirming the relevance of the multiseasonal information provided by Sentinel-2. Conducting RF classifications employing Sentinel-2 temporal information showed effectiveness in discriminating dominant vegetation cover, enabling the mapping of multiple levels of grassland condition, and thus facilitating the identification of degraded patches. Mapping critical areas that require restoration or conservation actions is imperative for managing biodiversity, as it offers valuable information to guide the prioritization of interventions, thus benefiting the conservation of native grasslands.

Data Availability

The data that support the findings of this study will be openly available in a public repository.

Conflicts of Interest

The authors declare that they have no conflicts of interest.

Authors' Contributions

Diego R. Guevara-Torres originally conceived the idea and collected the data, including fieldwork (vegetation sampling). Diego R. Guevara-Torres, José M. Facelli, and Bertram Ostendorf contributed to the study design. Diego R. Guevara-Torres and Bertram Ostendorf analyzed the data. The first draft of the manuscript was written by Diego R. Guevara-Torres with the advice of Bertram Ostendorf. All authors contributed critically to the drafts and gave final approval for publication.

Acknowledgments

We wish to thank Nicola Barnes and Kate Graham from the Murraylands and Riverland Landscape Board for their local knowledge and advice with the production of this manuscript. A special thanks to all the volunteers who participated in the fieldwork. This research was supported by the University of Adelaide International Postgraduate Scholarship Award. Transport to the study site was supported by the

Murraylands and Riverland Landscape Board from The Landscape Boards South Australia, as part of the grant “Increasing understanding of the dynamics of Iron-grass temperate grasslands to improve their management and conservation.” Open access publishing facilitated by the University of Adelaide, as part of the Wiley—The University of Adelaide agreement via the Council of Australian University Librarians.

References

- [1] C. Corbane, S. Lang, K. Pipkins et al., “Remote sensing for mapping natural habitats and their conservation status—new opportunities and challenges,” *International Journal of Applied Earth Observation and Geoinformation*, vol. 37, pp. 7–16, 2015.
- [2] S. Ferrier and V. Funk, “Mapping spatial pattern in biodiversity for regional conservation planning: where to from here?” *Systematic Biology*, vol. 51, no. 2, pp. 331–363, 2002.
- [3] Y. Xie, Z. Sha, and M. Yu, “Remote sensing imagery in vegetation mapping: a review,” *Journal of Plant Ecology*, vol. 1, no. 1, pp. 9–23, 2008.
- [4] V. Lawley, M. Lewis, K. Clarke, and B. Ostendorf, “Site-based and remote sensing methods for monitoring indicators of vegetation condition: an Australian review,” *Ecological Indicators*, vol. 60, pp. 1273–1283, 2016.
- [5] B. D. Sparrow, W. Edwards, S. E. M. Munroe et al., “Effective ecosystem monitoring requires a multi-scaled approach,” *Biological Reviews*, vol. 95, no. 6, pp. 1706–1719, 2020.
- [6] L. Royimani, O. Mutanga, J. Odindi, T. Dube, and T. N. Matongera, “Advancements in satellite remote sensing for mapping and monitoring of alien invasive plant species (AIPs),” *Physics and Chemistry of the Earth, Parts A/B/C*, vol. 112, pp. 237–245, 2019.
- [7] P. Macintyre, A. van Niekerk, and L. Mucina, “Efficacy of multi-season Sentinel-2 imagery for compositional vegetation classification,” *International Journal of Applied Earth Observation and Geoinformation*, vol. 85, Article ID 101980, 2020.
- [8] J. R. Xue and B. F. Su, “Significant remote sensing vegetation indices: a review of developments and applications,” *Journal of Sensors*, vol. 2017, Article ID 1353691, 17 pages, 2017.
- [9] Y. F. Xiao, W. J. Zhao, D. M. Zhou, and H. L. Gong, “Sensitivity analysis of vegetation reflectance to biochemical and biophysical variables at leaf, canopy, and regional scales,” *IEEE Transactions on Geoscience and Remote Sensing*, vol. 52, no. 7, pp. 4014–4024, 2014.
- [10] C. Shoko, O. Mutanga, and T. Dube, “Optimal season for discriminating C3 and C4 grass functional types using multi-date Sentinel 2 data,” *GIScience & Remote Sensing*, vol. 57, no. 1, pp. 127–139, 2020.
- [11] B. A. Bradley, “Remote detection of invasive plants: a review of spectral, textural and phenological approaches,” *Biological Invasions*, vol. 16, no. 7, pp. 1411–1425, 2014.
- [12] A. E. Maxwell, T. A. Warner, and F. Fang, “Implementation of machine-learning classification in remote sensing: an applied review,” *International Journal of Remote Sensing*, vol. 39, no. 9, pp. 2784–2817, 2018.
- [13] M. Belgiu and L. Drăguț, “Random forest in remote sensing: a review of applications and future directions,” *ISPRS Journal of Photogrammetry and Remote Sensing*, vol. 114, pp. 24–31, 2016.
- [14] E. W. Fox, R. A. Hill, S. G. Leibowitz, A. R. Olsen, D. J. Thornbrugh, and M. H. Weber, “Assessing the accuracy and stability of variable selection methods for random forest

- modeling in ecology,” *Environmental Monitoring and Assessment*, vol. 189, Article ID 316, 2017.
- [15] Y. Liu, W. Gong, X. Hu, and J. Gong, “Forest type identification with random forest using Sentinel-1A, Sentinel-2A, multi-temporal Landsat-8 and DEM data,” *Remote Sensing*, vol. 10, no. 6, Article ID 946, 2018.
- [16] Y. Cheng, A. Vrieling, F. Fava, M. Meroni, M. Marshall, and S. Gachoki, “Phenology of short vegetation cycles in a Kenyan rangeland from PlanetScope and Sentinel-2,” *Remote Sensing of Environment*, vol. 248, Article ID 112004, 2020.
- [17] W. J. Frampton, J. Dash, G. Watmough, and E. J. Milton, “Evaluating the capabilities of Sentinel-2 for quantitative estimation of biophysical variables in vegetation,” *ISPRS Journal of Photogrammetry and Remote Sensing*, vol. 82, pp. 83–92, 2013.
- [18] D. Phiri, M. Simwanda, S. Salekin, V. Nyirenda, Y. Murayama, and M. Ranagalage, “Sentinel-2 data for land cover/use mapping: a review,” *Remote Sensing*, vol. 12, no. 14, Article ID 2291, 2020.
- [19] M. E. D. Chaves, M. C. A. Picoli, and I. D. Sanches, “Recent applications of landsat 8/OLI and Sentinel-2/MSI for land use and land cover mapping: a systematic review,” *Remote Sensing*, vol. 12, no. 18, Article ID 3062, 2020.
- [20] J. Delegido, J. Verrelst, L. Alonso, and J. Moreno, “Evaluation of Sentinel-2 red-edge bands for empirical estimation of green LAI and chlorophyll content,” *Sensors*, vol. 11, no. 7, pp. 7063–7081, 2011.
- [21] J. Segarra, M. L. Buchailot, J. L. Araus, and S. C. Kefauver, “Remote sensing for precision agriculture: Sentinel-2 improved features and applications,” *Agronomy-Basel*, vol. 10, no. 5, Article ID 641, 2020.
- [22] Z. Gong, C. Zhang, L. Zhang, J. Bai, and D. Zhou, “Assessing spatiotemporal characteristics of native and invasive species with multi-temporal remote sensing images in the Yellow River Delta, China,” *Land Degradation & Development*, vol. 32, no. 3, pp. 1338–1352, 2021.
- [23] C. Jara, J. Delegido, J. Ayala, P. Lozano, A. Armas, and V. Flores, “Study of wetlands in the ecuadorian andes through the comparison of Landsat-8 and Sentinel-2 images,” *Revista De Teledetección*, no. 53, pp. 45–57, 2019.
- [24] N. Huber, C. Ginzler, R. Pazur et al., “Countrywide classification of permanent grassland habitats at high spatial resolution,” *Remote Sensing in Ecology and Conservation*, vol. 9, no. 1, pp. 133–151, 2023.
- [25] C. Tarantino, L. Forte, P. Blonda et al., “Intra-annual Sentinel-2 time-series supporting grassland habitat discrimination,” *Remote Sensing*, vol. 13, no. 2, Article ID 277, 2021.
- [26] D. Yan and K. M. de Beurs, “Mapping the distributions of C3 and C4 grasses in the mixed-grass prairies of southwest Oklahoma using the random forest classification algorithm,” *International Journal of Applied Earth Observation and Geoinformation*, vol. 47, pp. 125–138, 2016.
- [27] S. Rapinel, C. Mony, L. Lecoq, B. Clement, A. Thomas, and L. Hubert-Moy, “Evaluation of Sentinel-2 time-series for mapping floodplain grassland plant communities,” *Remote Sensing of Environment*, vol. 223, pp. 115–129, 2019.
- [28] M. Fauvel, M. Lopes, T. Dubo et al., “Prediction of plant diversity in grasslands using Sentinel-1 and -2 satellite image time series,” *Remote Sensing of Environment*, vol. 237, Article ID 111536, 2020.
- [29] Y. Zhao, Z. Liu, and J. Wu, “Grassland ecosystem services: a systematic review of research advances and future directions,” *Landscape Ecology*, vol. 35, no. 4, pp. 793–814, 2020.
- [30] I. C. Burke, W. K. Lauenroth, M. A. Vinton et al., “Plant-soil interactions in temperate grasslands,” *Biogeochemistry*, vol. 42, no. 1/2, pp. 121–143, 1998.
- [31] E. L. Fry, P. Manning, D. G. P. Allen et al., “Plant functional group composition modifies the effects of precipitation change on grassland ecosystem function,” *PLOS ONE*, vol. 8, no. 2, Article ID e57027, 2013.
- [32] D. E. Pearson, Y. K. Ortega, D. Villarreal et al., “The fluctuating resource hypothesis explains invasibility, but not exotic advantage following disturbance,” *Ecology*, vol. 99, no. 6, pp. 1296–1305, 2018.
- [33] D. Dahal, N. J. Pastick, S. P. Boyte, S. Parajuli, M. J. Oimoen, and L. J. Megard, “Multi-species inference of exotic annual and native perennial grasses in rangelands of the western United States using harmonized landsat and Sentinel-2 data,” *Remote Sensing*, vol. 14, no. 4, Article ID 807, 2022.
- [34] N. Williams, A. Marshall, and J. Morgan, *Land of Sweeping Plains: Managing and Restoring the Native Grasslands of South-Eastern Australia*, CSIRO Publishing, 2015.
- [35] C. S. Hallett, A. J. Hobday, J. R. Tweedley, P. A. Thompson, K. McMahon, and F. J. Valesini, “Observed and predicted impacts of climate change on the estuaries of south-western Australia, a Mediterranean climate region,” *Regional Environmental Change*, vol. 18, no. 5, pp. 1357–1373, 2018.
- [36] L. Ranghetti, M. Boschetti, F. Nutini, and L. Busetto, ““sen2r”: an R toolbox for automatically downloading and preprocessing Sentinel-2 satellite data,” *Computers & Geosciences*, vol. 139, Article ID 104473, 2020.
- [37] F. Gascon, C. Bouzinac, O. Thepaut et al., “Copernicus Sentinel-2A calibration and products validation status,” *Remote Sensing*, vol. 9, no. 6, Article ID 584, 2017.
- [38] G. Misra, F. Cawkwell, and A. Wingler, “Status of phenological research using Sentinel-2 data: a review,” *Remote Sensing*, vol. 12, no. 17, Article ID 2760, 2020.
- [39] C. Shoko and O. Mutanga, “Examining the strength of the newly-launched Sentinel 2 MSI sensor in detecting and discriminating subtle differences between C3 and C4 grass species,” *ISPRS Journal of Photogrammetry and Remote Sensing*, vol. 129, pp. 32–40, 2017.
- [40] H. A. Imran, D. Gianelle, D. Rocchini et al., “VIS-NIR, red-edge and nir-shoulder based normalized vegetation indices response to co-varying leaf and canopy structural traits in heterogeneous grasslands,” *Remote Sensing*, vol. 12, no. 14, Article ID 2254, 2020.
- [41] O. Löfgren, H. C. Prentice, T. Moeckel, B. C. Schmid, K. Hall, and D. Murrell, “Landscape history confounds the ability of the NDVI to detect fine-scale variation in grassland communities,” *Methods in Ecology and Evolution*, vol. 9, no. 9, pp. 2009–2018, 2018.
- [42] L. Breiman, “Random forests,” *Machine Learning*, vol. 45, no. 1, pp. 5–32, 2001.
- [43] M. B. Kursa and W. R. Rudnicki, “Feature selection with the boruta package,” *Journal of Statistical Software*, vol. 36, no. 11, pp. 1–13, 2010.
- [44] Y. Dickinson and D. A. Norton, “Divergent small-scale spatial patterns in New Zealand’s short tussock grasslands,” *New Zealand Journal of Ecology*, vol. 35, no. 1, pp. 76–82, 2011.
- [45] A. J. Rebelo, S. Gokool, P. B. Holden, and M. G. New, “Can Sentinel-2 be used to detect invasive alien trees and shrubs in savanna and grassland biomes?” *Remote Sensing Applications: Society and Environment*, vol. 23, Article ID 100600, 2021.
- [46] P. B. Holden, A. J. Rebelo, and M. G. New, “Mapping invasive alien trees in water towers: a combined approach using satellite

- data fusion, drone technology and expert engagement,” *Remote Sensing Applications: Society and Environment*, vol. 21, Article ID 100448, 2021.
- [47] T. I. Lenz and J. M. Facelli, “Correlations between environmental factors, the biomass of exotic annual grasses and the frequency of native perennial grasses,” *Australian Journal of Botany*, vol. 54, no. 7, pp. 655–667, 2006.
- [48] P. Lou, B. Fu, H. He et al., “An optimized object-based random forest algorithm for marsh vegetation mapping using high-spatial-resolution GF-1 and ZY-3 data,” *Remote Sensing*, vol. 12, no. 8, Article ID 1270, 2020.
- [49] E. R. Hunt Jr., C. S. T. Daughtry, J. U. H. Eitel, and D. S. Long, “Remote sensing leaf chlorophyll content using a visible band index,” *Agronomy Journal*, vol. 103, no. 4, pp. 1090–1099, 2011.
- [50] C. D. Elvidge and R. J. P. Lyon, “Influence of rock–soil spectral variation on the assessment of green biomass,” *Remote Sensing of Environment*, vol. 17, no. 3, pp. 265–279, 1985.